HHS Public Access

Author manuscript

Breast J. Author manuscript; available in PMC 2016 June 21.

Published in final edited form as:

Breast J. 2016 May ; 22(3): 264–273. doi:10.1111/tbj.12569.

Standardized Uptake Values from PET/MRI in Metastatic Breast Cancer: An Organ-based Comparison With PET/CT

Akshat C. Pujara, MD[*], **Roy A. Raad, MD**[*,†], **Fabio Ponzo, MD**[*,†], **Carolyn Wassong, MD**[*,‡], **James S. Babb, PhD**[*,§], **Linda Moy, MD**[*,‡,§], and **Amy N. Melsaether, MD**[*,‡,§]

[*]Department of Radiology, New York University School of Medicine, New York, New York

[†]Nuclear Medicine Section, New York University School of Medicine, New York, New York

[‡]Breast Imaging Section, New York University School of Medicine, New York, New York

[§]Center for Advanced Imaging Innovation and Research (CAI(2)R), NYU Department of Radiology, New York, New York

Abstract

Quantitative standardized uptake values (SUVs) from fluorine-18 (18F) fluorodeoxyglucose (FDG) positron emission tomography/computed tomography (PET/CT) are commonly used to evaluate the extent of disease and response to treatment in breast cancer patients. Recently, PET/magnetic resonance imaging (MRI) has been shown to qualitatively detect metastases from various primary cancers with similar sensitivity to PET/CT. However, quantitative validation of PET/ MRI requires assessing the reliability of SUVs from MR attenuation correction (MRAC) relative to CT attenuation correction (CTAC). The purpose of this retrospective study was to assess the utility of PET/MRI-derived SUVs in breast cancer patients by testing the hypothesis that SUVs derived from MRAC correlate well with those from CTAC. Between August 2012 and May 2013, 35 breast cancer patients (age 37–78 years, 1 man) underwent clinical 18F-FDG PET/CT followed by PET/MRI. One hundred seventy metastases were seen in 21 of 35 patients; metastases to bone in 16 patients, to liver in seven patients, and to nonaxillary lymph nodes in eight patients were sufficient for statistical analysis on an organ-specific per patient basis. SUVs in the most FDG-avid metastasis per organ per patient from PET/CT and PET/MRI were measured and compared using Pearson's correlations. Correlations between CTAC- and MRAC-derived SUVmax and SUVmean in 31 metastases to bone, liver, and nonaxillary lymph nodes were strong overall (ρ= 0.80, 0.81). SUVmax and SUVmean correlations were also strong on an organ-specific basis in 16 bone metastases (ρ= 0.76, 0.74), seven liver metastases (ρ= 0.85, 0.83), and eight nonaxillary lymph node metastases (ρ= 0.95, 0.91). These strong organ-specific correlations between SUVs from PET/CT and PET/MRI in breast cancer metastases support the use of SUVs from PET/MRI for quantitation of 18F-FDG activity.

Keywords

attenuation correction; breast cancer; hybrid imaging; PET/MRI; SUV

Address correspondence and reprint requests to: Amy N. Melsaether, MD, New York University School of Medicine, 560 First Avenue, New York, NY 10016, USA, or Amy.Melsaether@nyumc.org.

Evaluating disease extent and response to therapy in metastatic breast cancer often depends on accurate quantitation of fluorine-18 (18F) fluorodeoxyglucose (FDG) activity in positron emission tomography (PET), which requires attenuation correction. Computed tomography attenuation correction (CTAC) is based on tissue density information provided by CT (1). Signal from magnetic resonance imaging (MRI) is not dependent on tissue density, and thus the development of molecular MRI necessitates a different method for MR attenuation correction (MRAC). Current techniques for MRAC include the atlas-based method, which corrects images using a template data set, and the segmentation method, which assigns attenuation coefficients after tissue identification using standard reference values (2,3).

Potential benefits of molecular MRI include fusing PET and MR data in a single image acquisition, which may result in improved visualization of metastases without the additional ionizing radiation of CT (4). Qualitative validation of this new modality in terms of lesion detection is ongoing, and early results have been encouraging (5–26).

In addition to qualitative lesion detection, quantitative validation of MRAC is required before PET/MRI can be introduced into clinical practice, as standardized uptake values (SUVs) are often used to characterize suspicious lesions. This validation entails assessing SUVs and quantified lesion conspicuity from MRAC with CTAC as the reference standard. As such, the purpose of this study was to test the hypothesis that SUVs derived from MRAC correlate well with those from CTAC. Quantified PET conspicuity of breast cancer metastases from delayed PET/MRI was also compared with PET/CT.

MATERIALS AND METHODS

Written informed consent was obtained from all patients included in this institutional review board-approved, Health Insurance Portability and Accountability Act-compliant, retrospective study. Between August 2012 and May 2013, 35 consecutive breast cancer patients (mean age 58 ± 12 years, range 37–78 years; 34 women, 1 man) with known or suspected metastatic disease underwent whole-body PET/MRI following clinically indicated 18F-FDG PET/CT.

PET/CT Examination

Before imaging, patients fasted for at least 4 hours, insulin was withheld for 6 hours, and blood glucose was verified to be less than 200 mg/dL. Sixty ± fourteen minutes following intravenous 18F-FDG administration (mean dose 551 ± 18.5 MBq), patients underwent PET/CT from vertex to thighs (Siemens Biograph mCT); intravenous CT contrast agent was not administered except for in one patient per referring clinician. CT acquisition parameters were as follows: 120 kVp, 95 mA, 5.0 mm slice width, 50 cm transaxial field of view, 512 × 512 transaxial image matrix, B40f convolution kernel. PET acquisition parameters were as follows: 2 minutes per bed position, 814 mm transaxial field of view, 221 mm axial field of view, 200 ×200 transaxial matrix, and 3 mm Gaussian postreconstruction image filter. PET images were reconstructed with CT for attenuation correction with the attenuation-weighting ordered subsets expectation-maximization 3D algorithm at two iterations and 24 subsets.

With these parameters, the transaxial voxel size was 4.07 ×4.07 mm and the axial voxel size was 2.03 mm.

PET/MRI Examination

Immediately following PET/CT, patients were transferred to a nearby facility for PET/MRI. PET and MRI data were simultaneously acquired using the 3T Siemens Biograph mMR system 167 ± 36 minutes after the earlier 18F-FDG injection, with mean interval between start of PET/CT and start of PET/MRI of 106 ± 34 minutes. Whole-body PET/MRI examination was conducted from thighs to vertex and included 6–7 stations depending on patient height, with the following protocols per station: (i) 3D coronal volumetric interpolated breath-hold examination (VIBE) Dixon for MRAC; μ-maps were generated using an MR-based segmentation method, with separation of fat, soft tissue, lung, and background attenuation; (ii) T1-weighted radial 3D gradient-echo (radial VIBE); and (iii) 2D double-refocused echo-planar, diffusion weighted imaging (repetition time/echo time = 6000/ 65 ms, field of view 450 mm, 2.3 × 2.3 × 6.0 mm voxel, spectral attenuated inversion recovery fat-suppression, three diffusion directions [3-scan trace], and b-values 0, 350, and 700 second/mm^2). MR images were acquired with patients prone using a dedicated multichannel head and neck coil and a set of flexible body matrix coils. Rapid intravenous bolus injection of 0.1 mmol/L gadopentetate dimeglumine (Bayer Healthcare, Whippany, NJ, USA) per kg body weight was administered at 2.0 mL/second during the liver station. PET events were simultaneously accumulated for 6 minutes per station, for total examination time of approximately 45 minutes. The acquired PET sino-grams were reconstructed using the three-dimensional ordinary Poisson ordered-subset expectation-maximization algorithm (four iterations, 21 subsets), with incorporation of the u-maps from the attenuation correction scan.

Image Interpretation

A board-certified nuclear physician with 13 years of experience detected and characterized metastases from PET/CT scans using the MIM 5.4 fusion viewer (MIM Software, Cleveland, OH). A board-certified radiologist with 6 years of experience, including 18 months in PET/MRI, detected and characterized PET/MRI scans using XD3 software (version 3.6; Mirada Medical, Oxford, UK). Both readers used qualitative and quantitative PET findings for characterization of a suspicious lesion as a metastasis. Follow-up imaging, available in 28 patients at mean interval of 12 months (range 1–21), and prior studies, available in 33 patients at mean interval of 26 months (range 1–82), served as the reference standard. For 10 patients with less than 12 months of follow-up and prior imaging, and for patients with equivocal findings not clarified by follow-up and prior imaging, expert consensus between our institution’s most experienced PET and MRI readers served as the reference standard.

SUV Measurement

Following lesion detection, a single radiologist recorded SUVmax and SUVmean in a 1 cm^3 volume of interest (VOI) in breast cancer metastases and nine normal structures on PET/CT and PET/MRI; a 3 cm^3 VOI was used in normal liver. When multiple metastases were identified in the same organ in an individual patient, SUVs in the single most FDG-avid

metastasis were recorded to minimize any impact of patient-specific factors. Normal structures of interest were selected on the basis of their inclusion in recently published studies (5,9,14,27,28) or their particular relevance in breast cancer and included the following: axillary lymph nodes, bone (L4 vertebral body), breast (parenchyma), inguinal lymph nodes, liver (segment VII), lung (right lung at level of carina), mediastinal blood pool (right atrium), myocardium (left ventricular apex), psoas muscle (at level of L4 vertebral body), and subcutaneous fat (paraumbilical).

Statistical Analysis

Standardized uptake value ratios were calculated using normal liver as background and using normal tissue corresponding to the site of metastasis as background for the organ-specific analysis. Pearson's correlations (ρ) were used to characterize the relationship between MRAC- and CTAC-derived SUVs in all metastases and normal structures. Mixed model regression was used to assess the significance of the correlations to account for the lack of independence among results within patients with multiple metastatic sites. Mixed model ANOVA was performed to compare PET/ CT and PET/MRI in terms of SUVs and SUV ratios. An analogous evaluation of organ-specific metastases was performed utilizing Pearson's correlations and paired sample *t*-tests. ANOVA and post hoc paired *t*-tests were performed to compare metastatic sites and normal tissue in terms of the mean percent decrease of SUVs in between PET/CT and PET/MRI; percent decrease of SUVs was calculated as ([CTAC SUV – MRAC SUV]/ CTAC SUV) × 100. For these last comparisons, the sample was pared to patients with metastases to avoid confounding with interpatient differences.

Correlation $\rho > 0.70$ was considered strong, $0.30 \leq \rho \leq 0.70$ moderate, and $\rho < 0.30$ weak, similar to as described by Taylor (29). All statistical tests were conducted at the two-sided 5% significance level using SAS 9.3 software (SAS Institute, Cary, NC).

RESULTS

Breast Cancer Metastases

Of the 35 patients, 170 metastases were detected in 21 patients; 14 patients were free of metastatic disease on PET/CT and PET/MRI. Of the 21 patients with metastatic disease, index pathology was invasive ductal carcinoma in 15 patients, invasive lobular carcinoma in two patients, and was not specified in four patients. Metastases to bone, liver, and nonaxillary lymph node were frequent enough for statistical analysis. PET/MRI identified all patients with bone ($n = 16$), liver ($n = 7$), and nonaxillary lymph node ($n = 8$) metastases. PET/CT initially detected 15 patients with bone, six patients with liver, and eight patients with nonaxillary lymph node metastases. Upon unblinded review, the 16th patient with a bone metastasis and the 7th patient with liver metastases were identified on PET/CT with guidance from PET/ MRI.

SUVmax and SUVmean of metastases, with the most FDG-avid metastasis per organ per patient evaluated, demonstrated strong correlations between MRAC and CTAC overall (ρ=

0.80, 0.81). Correlations were also strong on an organ-specific basis in bone (ρ= 0.76, 0.74), liver (ρ= 0.85, 0.83), and non-axillary lymph node metastases (ρ= 0.95, 0.91).

Standardized uptake values of metastases from MRAC were not significantly different compared with CTAC overall. Similarly, no significant difference was seen on an organ-specific basis in metastases to bone and nonaxillary lymph node metastases. SUVs from MRAC were, however, significantly lower compared with CTAC in liver metastases. Table 1 summarizes the relationship between SUVs from PET/CT and PET/MRI in breast cancer metastases.

Normal Structures

Correlations and potential differences between CTAC- and MRAC-derived SUVmax and SUVmean in normal structures are listed in Table 2. In summary, correlations were strong for all normal structures combined (ρ= 0.79, 0.77). By organ, moderate correlations between SUVmax and/or SUVmean (ρ= 0.32–0.67) were seen in most normal structures, including axillary lymph nodes, breast, bone, inguinal lymph nodes, liver, lung, and psoas muscle. Correlations were strong in left ventricular myocardium (ρ= 0.83, 0.84) and weak in blood pool and subcutaneous fat (ρ= 0.15–0.23).

Standardized uptake values from MRAC were significantly lower compared with CTAC overall and in most individual normal structures, including axillary lymph nodes, blood pool, breast, bone, inguinal lymph nodes, liver, lung, and subcutaneous fat. SUVs from MRAC were significantly higher compared with CTAC in left ventricular myocardium. No significant difference was seen in psoas muscle.

PET Conspicuity Assessment

Using normal liver as background, metastasis/background SUV ratios were significantly higher from PET/MRI compared with PET/CT for metastases overall (SUVmax 3.88 ± 2.60 versus 2.02 ± 1.29, p = 0.001; SUVmean 4.80 ± 3.69 versus 2.17 ± 1.51, p = 0.001), bone metastases (SUVmax 3.34 ± 2.59 versus 1.73 ± 1.22, p = 0.01; SUVmean 4.21 ± 3.68 versus 1.74 ± 1.23, p = 0.008), liver metastases (SUV-max 2.98 ± 1.67 versus 2.32 ± 1.49, p = 0.001; SUVmean 3.85 ± 2.47 versus 2.72 ± 1.90, p = 0.004), and nonaxillary lymph node metastases (SUVmax 5.74 ± 2.61 versus 2.32 ± 1.27, p = 0.002; SUVmean 6.81 ± 4.24 versus 2.53 ± 1.60, p = 0.006).

Using normal tissue corresponding to the site of metastasis as background, metastasis/background SUVmax and SUVmean ratios were also significantly higher from PET/MRI compared with PET/CT for metastases overall ($p \leq 0.05$), liver metastases ($p \leq 0.004$), and nonaxillary lymph node metastases ($p \leq 0.02$). However, no significant difference was seen in SUVmax and SUVmean ratios of bone metastases/normal bone between PET/MRI and PET/CT ($p \geq 0.43$) (Fig. 1).

Figure 2 illustrates the mean percent decrease of SUVmax and SUVmean in all metastases combined and on an organ-specific basis in the interval between PET/CT and PET/MRI; corresponding differences in normal tissue are also shown. Mean percent decrease was significantly lower in 31 total metastases in 21 patients compared with corresponding

normal tissue in the same patients after 101 ± 31 minutes ($p \leq 0.005$). On an organ-specific basis, mean percent decrease was significantly lower in seven liver metastases in seven different patients compared with normal liver in the same patients after 90 ± 31 minutes ($p \leq 0.008$) and in eight nonaxillary lymph node metastases in eight different patients compared with normal lymph nodes in the same patients after 112 ± 39 minutes ($p < 0.001$). Meanwhile, mean percent decrease of SUVmax and SUVmean was not significantly different between 16 bone metastases in 16 different patients and normal bone in the same patients after 97 ± 23 minutes ($p \geq 0.85$).

DISCUSSION

Our study shows that SUVs from PET/MRI correlate well with those from PET/CT and supports the use of PET/MRI-derived SUVs in metastatic breast cancer for quantitation of organ-specific 18F-FDG activity. The detection and monitoring of breast cancer metastases is important because it has potential to change patient treatment. Currently, there is no reliable blood test to detect the presence of metastases. PET/CT, bone scan, and liver CT are the most common imaging tests used to detect metastatic disease. Thus far, PET/MRI has shown comparable performance to PET/CT for lesion detection (5⁻24،26) and quantitative measures (5⁻9،11،12،14،16،19،22،23،27، 28) in oncologic populations. Without the CT radiation of PET/CT, PET/MRI may have a role in patients undergoing serial examinations, and also in cases requiring more detailed information about the breast or brain than CT can provide. Here, we investigate quantitative measures of PET/MRI specifically in breast cancer metastases to common sites including bone, liver, and nonaxillary lymph nodes.

SUVs from PET/MRI in Breast Cancer

Correlations—This study separates metastases by organs of particular relevance in breast cancer, namely bone, liver, and nonaxillary lymph nodes, and shows strong correlations between MRAC- and CTAC-derived SUVs in these disease- and organ-specific metastases. The inclusion of a single metastasis per organ per patient in this study mitigates patient-specific biologic variability. These findings add to the recent work by Pace et al. (9), which showed strong correlations between SUVs from PET/MRI and PET/ CT in 35 lymph node and 14 grouped distant breast cancer metastases (11 bone, 3 lung). Our findings also agree with recent publications that showed strong correlations for metastases overall (5،8،14), in head and neck cancer (6) and in pediatric populations (12).

Magnetic resonance attenuation correction- and CTAC-derived SUVs in normal structures have been shown to correlate well, further supporting the use of SUVs from PET/MRI clinically, noting that organ-specific reproducibility has been somewhat inconsistent (5،8،9،17،27). Differences between correlations are likely multifactorial and related to small sample sizes, variable intervals between radiotracer injection and PET imaging, and different durations of PET event accumulation, as summarized in Table 3. The inherent difficulty of reproducing SUVs should also be considered (30،31).

Absolute Differences—In this study, MRAC-derived SUVs in metastases were not significantly different compared with CTAC-derived SUVs in bone and non-axillary lymph nodes but were lower than CTAC-derived SUVs in liver. Meanwhile, SUVs in all normal

structures except psoas muscle were lower on PET/MRI compared with PET/CT. These findings suggest slower washout of radiotracer from metastases compared with normal structures and are consistent with prior studies assessing SUVs at two time points (32–37). Two recent studies reported lower SUVs in distant mixed metastases on PET/MRI compared with PET/CT (8,14), while two additional studies found higher SUVs in distant mixed and breast cancer metastases, respectively (5,9). These disparities among metastases may be partially attributable to examination timing and to variable types and sites of metastatic disease.

Quantified PET Conspicuity

Similar to Al-Nabhani et al. and Wiesmuller et al., we found increased metastasis/liver SUV ratios on PET/MRI compared with PET/CT overall (5,14) and also when we stratified metastases by organ. While liver, blood pool, and muscle are often used as background when calculating metastasis/background SUV ratios (38), organ-based SUV ratios may improve lesion characterization, as detection of a metastasis often depends on comparing a suspicious lesion to the normal surrounding parent organ (39).

To this end, we also assessed objective PET contrast on PET/MRI and PET/CT using normal tissue corresponding to the site of metastasis as background. While bone metastasis/normal liver SUV ratios were higher on PET/MRI, bone metastasis/normal bone SUV ratios were not significantly different between PET/CT and PET/MRI. The latter result is concordant with there being no difference between the mean percent decrease of SUVs of bone metastases and that of normal bone in the interval between PET/CT and PET/MRI and the similar qualitative conspicuity of bone metastases on PET/CT and PET/ MRI in this study (Fig. 3). Meanwhile, the higher metastasis/corresponding normal tissue SUV ratios observed in liver and nonaxillary lymph node metastases on PET/MRI are also concordant with the lower percent decrease of SUVs in metastases to these organs compared with corresponding normal tissue; as a larger percentage of radiopharmaceutical had cleared from normal tissue compared with metastases in these organs, qualitative lesion conspicuity was increased (Figs 4 and 5).

Bone, liver, and lymph nodes represent three of the most common sites of breast cancer metastases, with osseous metastases occurring first in up to 50% of patients (40). Accurate detection of metastases to these organs is thus critical for appropriate staging and follow-up. Improved visualization and characterization of liver and nonaxillary lymph metastases on PET/MRI in this study may be related to delayed imaging as demonstrated in previous dual time point imaging studies using the same scanner (32–35,37,41,42). However, the finding of similar quantified conspicuity of bone metastases on PET/CT and delayed PET/MRI suggests that organ-specific factors may play a role in lesion detection. The impact of scanner-specific variables also remains undetermined, and additional studies reversing the order of PET/MRI and PET/CT may help determine the role of image timing and scanner-specific factors to organ-specific changes in PET conspicuity. Such studies may ultimately aid in tailoring examination timings for organ-specific lesion detection and follow-up.

Limitations

The primary limitation of this study was the delay between PET/CT and PET/MRI. However, our findings of good correlations between SUVs in breast cancer metastases and normal structures from PET/MRI and PET/CT are independent of this delay and validate the use of PET/MRI in the setting of metastatic breast cancer. The time interval between examinations was somewhat variable between patients, and physiologic clearance of radiotracer during the interval between PET/CT and PET/MRI potentially confounds results (31›43). Findings regarding the metabolic activity of metastases using PET/MRI in the current study are also considered preliminary due to the small sample size. While assessing one metastasis per organ per patient may have limited the impact of patient-specific factors, it led to a relatively small number of metastases evaluated.

CONCLUSION

Our study supports the clinical use of quantitative SUVs measured on PET/MRI by demonstrating strong organ-specific correlations between SUVs in breast cancer metastases to bone, liver, and nonaxillary lymph nodes derived from PET/MRI and from PET/ CT and by showing that SUVs in normal structures correlate well in breast cancer patients. Changes in quantified PET conspicuity of breast cancer metastases appear to be organ-specific, and further investigation may allow examinations to be tailored to maximize lesion detection at specific sites of breast cancer metastases. Additional studies may be helpful to determine if quantitation of SUVs and MR imaging features of PET/MRI allow for further characterization of suspected metastases, especially in the liver, bone, and nonaxillary lymph nodes.

References

1. Visvikis D, Costa DC, Croasdale I, et al. CT-based attenuation correction in the calculation of semi-quantitative indices of [18F]FDG uptake in PET. Eur J Nucl Med Mol Imaging. 2003; 30:344–53. [PubMed: 12634961]
2. Zaidi H, Montandon ML, Slosman DO. Magnetic resonance imaging-guided attenuation and scatter corrections in three-dimensional brain positron emission tomography. Med Phys. 2003; 30:937–48. [PubMed: 12773003]
3. Hofmann M, Bezrukov I, Mantlik F, et al. MRI-based attenuation correction for whole-body PET/MRI: quantitative evaluation of segmentation- and atlas-based methods. J Nucl Med. 2011; 52:1392–9. [PubMed: 21828115]
4. Yoon SH, Goo JM, Lee SM, Park CM, Seo HJ, Cheon GJ. Positron emission tomography/magnetic resonance imaging evaluation of lung cancer: current status and future prospects. J Thorac Imaging. 2014; 29:4–16. [PubMed: 24296699]
5. Al-Nabhani KZ, Syed R, Michopoulou S, et al. Qualitative and quantitative comparison of PET/CT and PET/MR imaging in clinical practice. J Nucl Med. 2014; 55:88–94. [PubMed: 24337608]
6. Boss A, Stegger L, Bisdas S, et al. Feasibility of simultaneous PET/MR imaging in the head and upper neck area. Eur Radiol. 2011; 21:1439–46. [PubMed: 21308378]
7. Chandarana H, Heacock L, Rakheja R, et al. Pulmonary nodules in patients with primary malignancy: comparison of hybrid PET/MR and PET/CT imaging. Radiology. 2013; 268:874–81. [PubMed: 23737537]
8. Drzezga A, Souvatzoglou M, Eiber M, et al. First clinical experience with integrated whole-body PET/MR: comparison to PET/CT in patients with oncologic diagnoses. J Nucl Med. 2012; 53:845–55. [PubMed: 22534830]

9. Pace L, Nicolai E, Luongo A, et al. Comparison of whole-body PET/CT and PET/MRI in breast cancer patients: lesion detection and quantitation of 18F-deoxyglucose uptake in lesions and in normal organ tissues. Eur J Radiol. 2014; 83:289–96. [PubMed: 24331845]
10. Platzek I, Beuthien-Baumann B, Schneider M, et al. PET/ MRI in head and neck cancer: initial experience. Eur J Nucl Med Mol Imaging. 2013; 40:6–11. [PubMed: 23053322]
11. Rauscher I, Eiber M, Fürst S, et al. PET/MR imaging in the detection and characterization of pulmonary lesions: technical and diagnostic evaluation in comparison to PET/CT. J Nucl Med. 2014; 55:724–9. [PubMed: 24652827]
12. Schäfer JF, Gatidis S, Schmidt H, et al. Simultaneous whole-body PET/MR imaging in comparison to PET/CT in pediatric oncology: initial results. Radiology. 2014; 273:220–31. [PubMed: 24877983]
13. Schwenzer N, Schrami C, Müller M, et al. Pulmonary lesion assessment: comparison of whole-body hybrid MR/PET and PET/ CT imaging–pilot study. Radiology. 2012; 264:551–8. [PubMed: 22653189]
14. Wiesmuller M, Quick HH, Navalpakkam B, et al. Comparison of lesion detection and quantitation of tracer uptake between PET from a simultaneously acquiring whole-body PET/MR hybrid scanner and PET from PET/CT. Eur J Nucl Med Mol Imaging. 2013; 40:12–21. [PubMed: 23053323]
15. Beiderwellen K, Huebner M, Heusch P, et al. Whole-body [^{18}F]FDG PET/MRI vs. PET/CT in the assessment of bone lesions in oncological patients: initial results. Eur Radiol. 2014; 24:2023–30. [PubMed: 24907940]
16. Eiber M, Takei T, Souvatzoglou M, et al. Performance of whole-body integrated 18F-FDG PET/MR in comparison to PET/CT for evaluation of malignant bone lesions. J Nucl Med. 2014; 55:191–7. [PubMed: 24309383]
17. Heusch P, Nensa F, Schaarschmidt B, et al. Diagnostic accuracy of whole-body PET/MRI and whole-body PET/CT for TNM staging in oncology. Eur J Nucl Med Mol Imaging. 2015; 42:42–8. [PubMed: 25112399]
18. Huellner MW, Appenzeller P, Kuhn FP, et al. Whole-body nonenhanced PET/MR versus PET/CT in the staging and restaging of cancers: preliminary observations. Radiology. 2014; 273:859–69. [PubMed: 25102372]
19. Jeong JH, Cho IH, Kong EJ, Chun KA. Evaluation of dixon sequence on hybrid PET/MR compared with contrast-enhanced PET/CT for PET-positive lesions. Nucl Med Mol Imaging. 2014; 48:26–32. [PubMed: 24900135]
20. Kuhn FP, Crook DW, Mader CE, Appenzeller P, von Schulthess GK, Schmid DT. Discrimination and anatomical mapping of PET-positive lesions: comparison of CT attenuation-corrected PET images with coregistered MR and CT images in the abdomen. Eur J Nucl Med Mol Imaging. 2013; 40:44–51. [PubMed: 22955547]
21. Kuhn FP, Hullner M, Mader CE, et al. Contrast-enhanced PET/MR imaging versus contrast-enhanced PET/CT in head and neck cancer: how much MR information is needed? J Nucl Med. 2014; 55:551–8. [PubMed: 24491410]
22. Partovi S, Kohan A, Vercher-Conejero JL, et al. Qualitative and quantitative performance of 18F-FDG-PET/MRI versus 18F-FDG-PET/CT in patients with head and neck cancer. AJNR Am J Neuroradiol. 2014; 35:1970–5. [PubMed: 24924545]
23. Varoquaux A, Rager O, Poncet A, et al. Detection and quantification of focal uptake in head and neck tumours: (18)F-FDG PET/MR versus PET/CT. Eur J Nucl Med Mol Imaging. 2014; 41:462–75. [PubMed: 24108458]
24. Taneja S, Jena A, Goel R, Sarin R, Kaul S. Simultaneous whole-body 18F-FDG PET-MRI in primary staging of breast cancer: a pilot study. Eur J Radiol. 2014; 83:2231–9. [PubMed: 25282709]
25. Nensa F, Tezgah E, Poeppel TD, et al. Integrated 18F-FDG-PET/MRI in the assessment of cardiac masses: a pilot study. J Nucl Med. 2015; 56:255–60. [PubMed: 25552667]
26. Fraioli F, Screaton N, Janes S, et al. Non-small-cell lung cancer resectability: diagnostic value of PET/MR. Eur J Nucl Med Mol Imaging. 2015; 42:49–55. [PubMed: 25120040]

27. Kershah S, Partovi S, Traughber BJ, et al. Comparison of standardized uptake values in normal structures between PET/CT and PET/MRI in an oncology patient population. Mol Imaging Biol. 2013; 15:776–85. [PubMed: 23632951]
28. Heusch P, Buchbender C, Beiderwellen K, et al. Standardized uptake values for [^{18}F] FDG in normal organ tissues: comparison of whole-body PET/CT and PET/MRI. Eur J Radiol. 2013; 82:870–6. [PubMed: 23394765]
29. Taylor R. Interpretation of the correlation coefficient: a basic review. J Diagn Med Sonogr. 1990; 1:35–9.
30. Scheuermann JS, Saffer JR, Karp JS, Levering AM, Siegel BA. Qualification of PET scanners for use in multicenter cancer clinical trials: the American College Of Radiology Imaging Network Experience. J Nucl Med. 2009; 50:1187–93. [PubMed: 19525463]
31. Westerterp M, Pruim J, Oyen W, et al. Quantification of FDG PET studies using standardised uptake values in multi-centre trials: effects of image reconstruction, resolution and ROI definition parameters. Eur J Nucl Med Mol Imaging. 2007; 34:392–404. [PubMed: 17033848]
32. Basu S, Alavi A. Partial volume correction of standardized uptake values and the dual time point in FDG-PET imaging: should these be routinely employed in assessing patients with cancer? Eur J Nucl Med Mol Imaging. 2007; 34:1527–9. [PubMed: 17522857]
33. Boerner AR, Weckesser M, Herzog H, et al. Optimal scan time for fluorine-18 fluorodeoxyglucose positron emission tomography in breast cancer. Eur J Nucl Med. 1999; 26:226–30. [PubMed: 10079312]
34. Hustinx R, Smith RJ, Benard F, et al. Dual time point fluorine-18 fluorodeoxyglucose positron emission tomography: a potential method to differentiate malignancy from inflammation and normal tissue in head and neck. Eur J Nucl Med. 1999; 26:1345–8. [PubMed: 10541835]
35. Kumar R, Loving VA, Chauhan A, Zhuang H, Mitchell S, Alavi A. Potential of dual-time-point imaging to improve breast cancer diagnosis with 18F-FDG-PET. J Nucl Med. 2005; 46:1819–24. [PubMed: 16269595]
36. Lee J, Kim SK, Lee SM, Moon SH, Kim TS. Detection of hepatic metastases using dual-time-point FDG PET/CT scans in patients with colorectal cancer. Mol Imaging Biol. 2011; 13:565–72. [PubMed: 20683670]
37. Mavi A, Urhan M, Yu JQ, et al. Dual time point 18F-FDG PET imaging detects breast cancer with high sensitivity and correlates well with histologic subtypes. J Nucl Med. 2006; 47:1440–6. [PubMed: 16954551]
38. Tylski P, Stute S, Grotus N, et al. Comparative assessment of methods for estimating tumor volume and standardized uptake value in (18)F-FDG PET. J Nucl Med. 2010; 51:268–76. [PubMed: 20080896]
39. Boktor RR, Walker G, Stacey R, Gledhill S, Pitman AG. Reference range for intrapatient variability in blood-pool and liver SUV for 18F-FDG PET. J Nucl Med. 2013; 54:677–82. [PubMed: 23512357]
40. Gaeta CM, Vercher-Conejero JL, Sher AC, Kohan A, Rub-bert C, Avril N. Recurrent and metastatic breast cancer PET, PET/ CT, PET/MRI: FDG and new biomarkers. Q J Nucl Med Mol Imaging. 2013; 57:352–66. [PubMed: 24322792]
41. Xiu Y, Bhutani C, Dhurairaj T, et al. Dual-time point FDG-PET imaging in the evaluation of pulmonary nodules with minimally increased metabolic activity. Clin Nucl Med. 2007; 32:101–5. [PubMed: 17242561]
42. Matthies A, Hickeson M, Cuchiara A, Alavi A. Dual-time-point 18F-FDG PET for the evaluation of pulmonary nodules. J Nucl Med. 2002; 43:871–5. [PubMed: 12097455]
43. Thie J. Understanding the standardized uptake value, its methods, and implications for usage. J Nucl Med. 2004; 45:1431–4. [PubMed: 15347707]

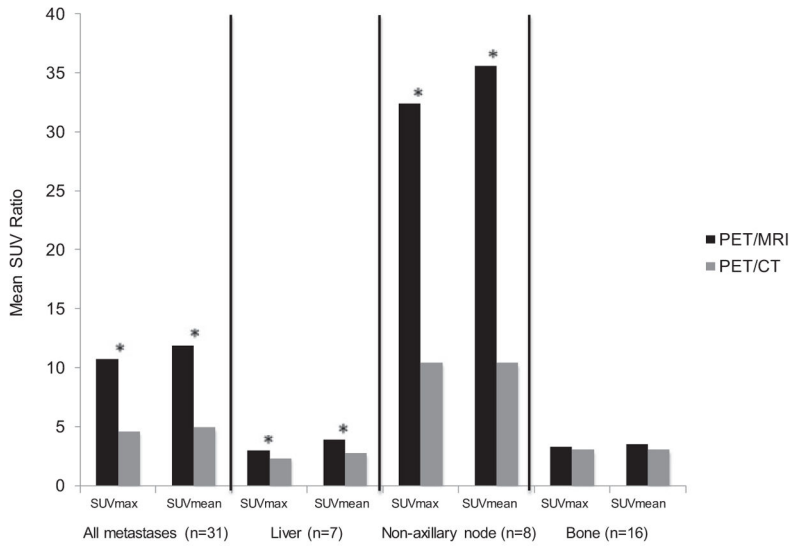

Figure 1.

SUV ratios of metastases/corresponding normal tissue from PET/MRI and PET/CT. *Statistically significant. In contrast to when normal liver was used as background, no significant difference was seen in SUV ratios of bone metastases/normal bone.

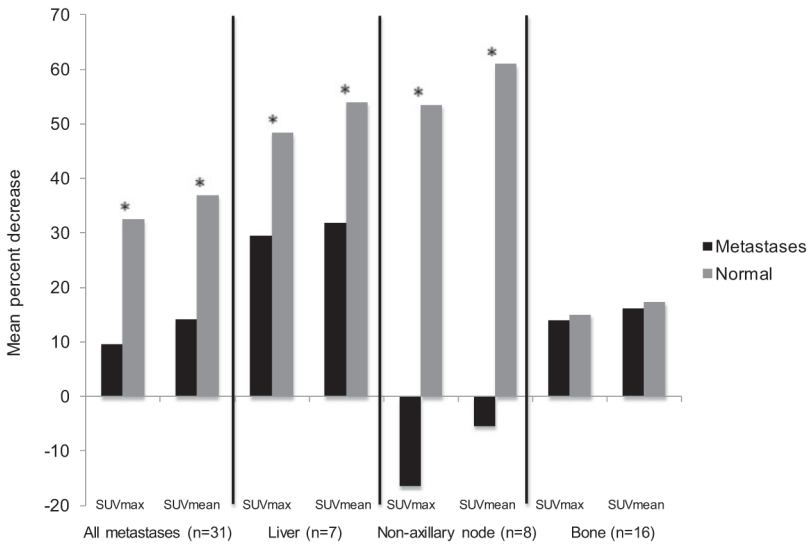

Figure 2.

Mean percent decrease of SUVs in metastases and corresponding normal tissue in interval between PET/CT and PET/ MRI. *Statistically significant. No significant difference was seen in the mean percent decrease of SUVs in bone metastases compared with normal bone.

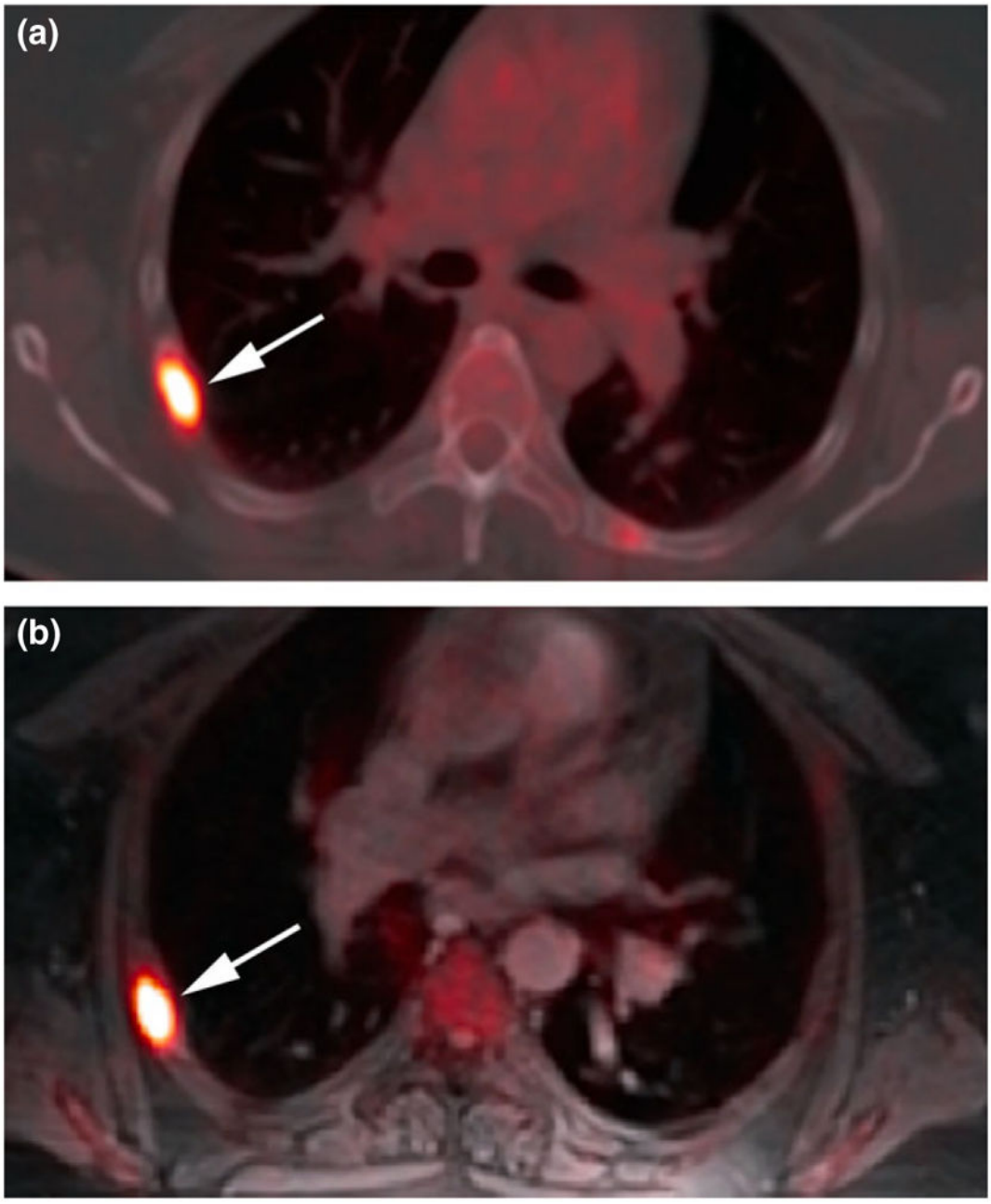

Figure 3.
(a) Right posterolateral fifth rib metastasis on axial 18F-FDG PET/CT (unenhanced). (b) Similar conspicuity on axial 18F-FDG PET/MRI (radial volumetric interpolated breath-hold examination) at later scan time.

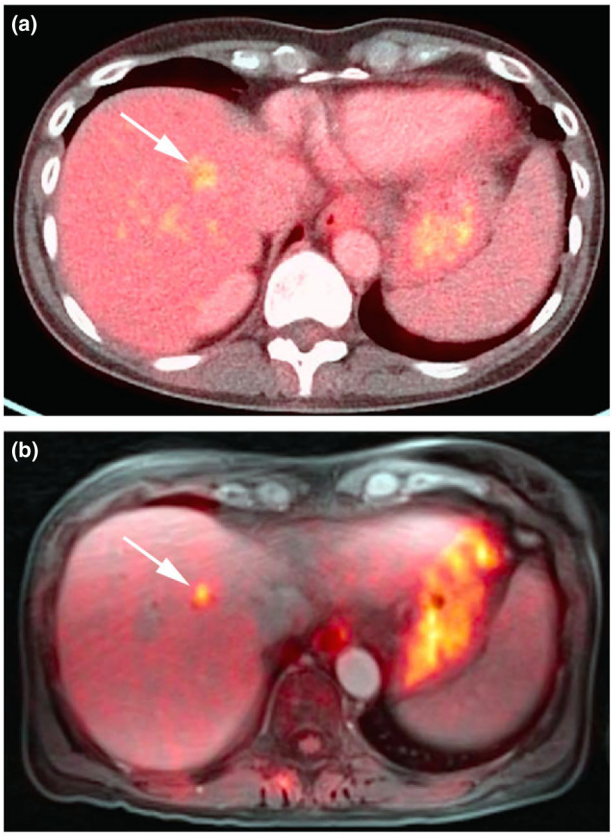

Figure 4.
(a) Liver metastasis on axial 18F-FDG PET/CT (contrast-enhanced). (b) Increased conspicuity on axial 18F-FDG PET/ MRI (radial volumetric interpolated breath-hold examination) at later scan time.

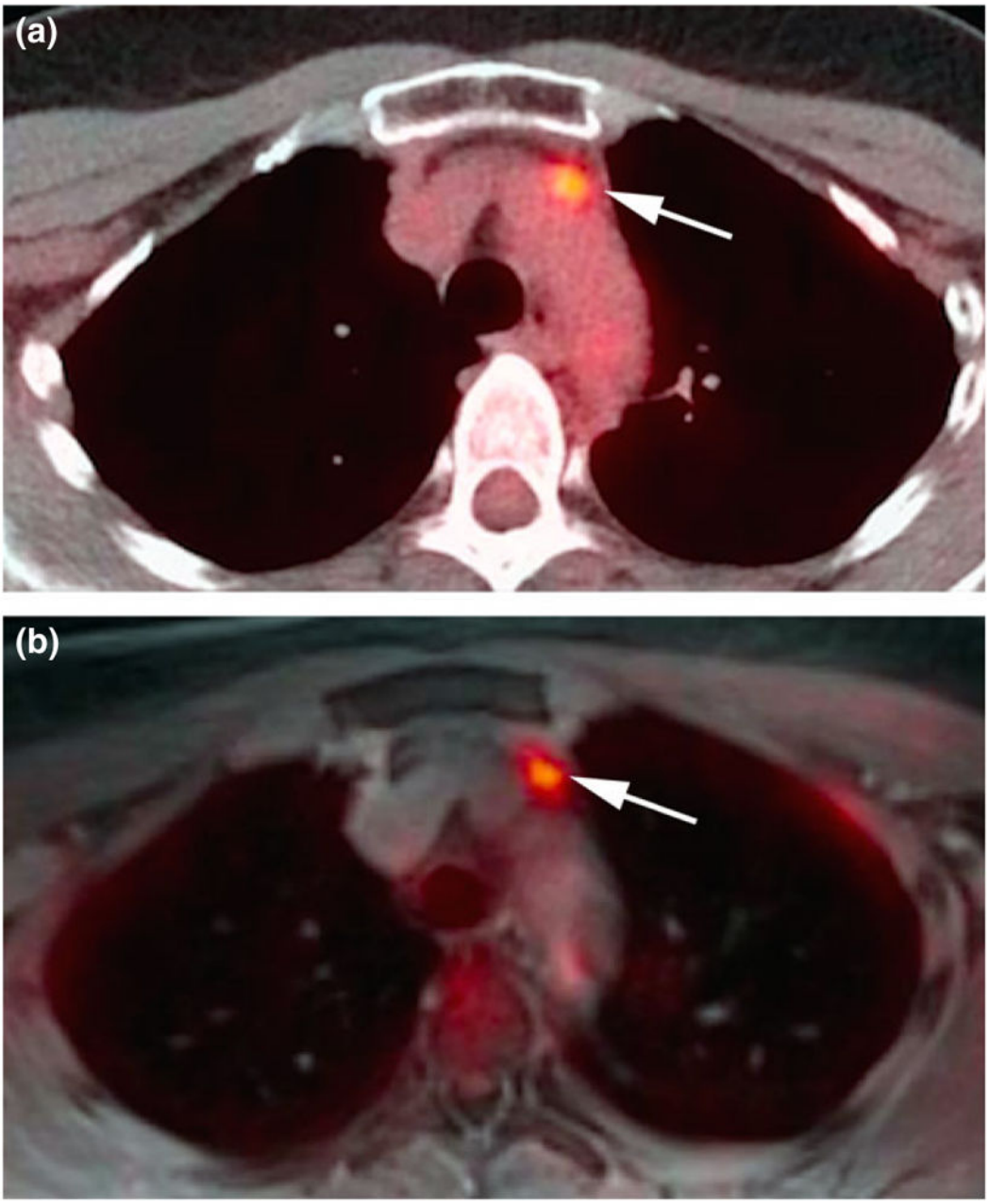

Figure 5.
(a) Prevascular lymph node metastasis on axial 18F-FDG PET/CT (unenhanced). (b) Increased conspicuity on axial 18F-FDG PET/MRI (radial volumetric interpolated breath-hold examination) at later scan time.

Table 1

Correlations and Potential Differences between Standardized Uptake Values in Breast Cancer Metastases from PET/CT * and PET/MRI (mean ± SD)

Site	No.	Measure	PET/CT	PET/MR	Correlation ρ(p)	t-test † p
All	31	SUVmax	6.99 ± 4.63	6.25 ± 4.91	0.80 (<0.001)	0.15
		SUVmean	5.76 ± 3.89	4.92 ± 3.88	0.81 (<0.001)	0.07
Bone	16	SUVmax	5.89 ± 3.92	4.89 ± 3.61	0.76 (<0.001)	0.15
		SUVmean	4.59 ± 2.86	3.79 ± 2.61	0.74 (<0.001)	0.12
Liver	7	SUVmax	7.79 ± 5.78	4.96 ± 3.04	0.85 (0.01)	0.05
		SUVmean	6.74 ± 4.89	4.20 ± 2.64	0.83 (0.01)	0.03
Lymph node	8	SUVmax	8.48 ± 4.93	10.08 ± 6.69	0.95 (<0.001)	0.12
		SUVmean	7.25 ± 4.50	7.83 ± 5.57	0.91 (<0.001)	0.52

*A bone metastasis in one patient and liver metastases in a different patient were initially not seen on PET/CT.

†t-test describes level of significance of difference between PET/CT and PET/MRI standardized uptake values.

Table 2

Correlations and Potential Differences between Standardized Uptake Values in Normal Structures from PET/CT and PET/MRI (mean ± SD; $n = 35^{*}$)

Structure	Measure	PET/CT	PET/MRI	Pearson's correlation ρ(p)	t-test† p
All structures	SUVmax	1.60 ± 1.35	1.15 ± 1.37	0.79 (<0.001)	<0.001
	SUVmean	1.31 ± 1.12	0.90 ± 1.13	0.77 (<0.001)	<0.001
Axillary node	SUVmax	0.71 ± 0.22	0.51 ± 0.21	0.24 (NS)	<0.001
	SUVmean	0.56 ± 0.15	0.38 ± 0.16	0.35 (0.04)	<0.001
Blood pool	SUVmax	2.39 ± 0.53	0.85 ± 0.27	0.22 (NS)	<0.001
	SUVmean	2.12 ± 0.45	0.67 ± 0.21	0.15 (NS)	<0.001
Bone	SUVmax	2.39 ± 0.75	2.00 ± 0.70	0.67 (<0.001)	<0.001
	SUVmean	1.98 ± 0.63	1.59 ± 0.56	0.60 (<0.001)	<0.001
Breast	SUVmax	0.96 ± 0.36	0.51 ± 0.23	0.37 (0.04)	<0.001
	SUVmean	0.75 ± 0.30	0.40 ± 0.22	0.36 (0.04)	<0.001
Inguinal node	SUVmax	0.81 ± 0.19	0.48 ± 0.22	0.24 (NS)	<0.001
	SUVmean	0.65 ± 0.15	0.35 ± 0.21	0.35 (0.04)	<0.001
Liver	SUVmax	3.54 ± 0.63	1.83 ± 0.62	0.33 (0.05)	<0.001
	SUVmean	2.74 ± 0.47	1.25 ± 0.47	0.23 (NS)	<0.001
Lung	SUVmax	0.64 ± 0.18	0.34 ± 0.11	0.22 (NS)	<0.001
	SUVmean	0.55 ± 0.16	0.28 ± 0.09	0.36 (0.03)	<0.001
Myocardium	SUVmax	3.26 ± 2.20	4.03 ± 2.53	0.83 (<0.001)	0.004
	SUVmean	2.69 ± 1.92	3.34 ± 2.09	0.84 (<0.001)	0.003
Psoas muscle	SUVmax	0.90 ± 0.17	0.90 ± 0.34	0.29 (NS)	NS
	SUVmean	0.76 ± 0.13	0.71 ± 0.28	0.32 (0.05)	NS
Subcutaneous fat	SUVmax	0.46 ± 0.17	0.26 ± 0.14	0.21 (NS)	<0.001
	SUVmean	0.35 ± 0.13	0.18 ± 0.10	0.23 (NS)	<0.001

*n = 30 for breast tissue secondary to bilateral mastectomy in five patients.

†t-test describes level of significance of difference between PET/CT and PET/MRI standardized uptake values.

NS, not significant.

Breast J. Author manuscript; available in PMC 2016 June 21.

Table 3

Studies Comparing CTAC- and MRAC-Derived Standardized Uptake Values in Normal Structures

	Drzezga (8)	Heusch (28)	Kershah (27)	Pace (9)	Current study
Primary malignancy	Various	Various	Various	Breast	Breast
Number of patients	32	25	40	36	35
Injection-PET/CT interval (mean ± SD)	86 ± 8 min	60 min	66 ± 7 min	60 ± 10 min	60 ± 14 min
PET accumulation time per station (PET/CT)	2 min	2 min	1.5–2 min	1.5 min	2 min
PET/MRI manufacturer	Siemens	Siemens	Philips	Siemens	Siemens
Injection-PET/MRI interval (mean ± SD)	140 ± 24 min	152 ± 42 min	117 ± 15 min	148 ± 22 min	167 ± 36 min
PET accumulation time per station (PET/MRI)	4 min	8 min	2–2.5 min	4 min	6 min
MRAC segmentation classes	4	4	3	4	4
SUV relationships [*,†]					
Blood pool					
Correlation	NE	Weak	Moderate	NE	Weak
Difference	NE	MRAC<CTAC	MRAC<CTAC	NE	MRAC<CTAC
Bone					
Correlation	Moderate (mean)	Moderate	Strong	NE	Moderate
Difference	MRAC<CTAC	MRAC<CTAC (max)	MRAC>CTAC	NE	MRAC<CTAC
Lung					
Correlation	Moderate (mean)	Weak	Strong (max)	Moderate	Moderate (mean)
Difference	MRAC<CTAC	MRAC<CTAC	No difference	MRAC<CTAC	MRAC<CTAC
Liver					
Correlation	Moderate (mean)	Strong (mean)	Moderate	Moderate	Moderate (max)
Difference	MRAC<CTAC	MRAC<CTAC	MRAC<CTAC (mean)	MRAC<CTAC	MRAC<CTAC
Myocardium					
Correlation	NE	Strong	Strong	Strong	Strong
Difference	NE	MRAC>CTAC (max)	MRAC>CTAC	MRAC>CTAC	MRAC>CTAC
Noncardiac muscle					
Correlation	Weak (mean)	Moderate (max)	Moderate	Moderate	Moderate (mean)
Difference	MRAC<CTAC	MRAC<CTAC	MRAC>CTAC (max)	MRAC<CTAC	No difference
Fat					

	Drzezga (8)	Heusch (28)	Kershah (27)	Pace (9)	Current study
Correlation	NE	Moderate (mean)	Moderate	NE	Weak
Difference	NE	MRAC<CTAC	No difference	NE	MRAC<CTAC

*SUVmax and SUVmean unless indicated.

†Correlation $\rho > 0.70$ was considered strong, $0.30 \leq \rho \leq 0.70$ moderate, and $\rho < 0.30$ weak.

NE, not evaluated.